

Impact of queue feedback on the stability and dynamics of a Rate Control Protocol (RCP) with two delays

Abuthahir, Gaurav Raina

Department of Electrical Engineering, Indian Institute of Technology Madras, Chennai - 600 036, India

Abstract

Rate Control Protocol (RCP) uses feedback from routers to assign flows their fair rate. RCP estimates the fair rate using two forms of feedback: rate mismatch and queue size. An outstanding design question for RCP is whether the queue size feedback is useful or not. To address this, we analyze stability and the bifurcation properties of RCP in both the cases i.e., with and without queue size feedback. The model considers flows with two different round-trip times, operating over a single bottleneck link. By using an exogenous bifurcation parameter, we show that the system loses stability via a Hopf bifurcation and hence we can expect a limit cycle branching from the fixed point. We highlight that the presence of queue feedback can readily destabilize the system. Using Poincarè normal forms and the center manifold theorem, we show that the Hopf bifurcation is super-critical in the case of RCP without queue feedback. Whereas, in the presence of queue feedback, we show that the system can undergo a sub-critical Hopf bifurcation for some parameter values. A sub-critical Hopf bifurcation can result in either large amplitude limit cycles or unstable limit cycles, and hence should be avoided in engineering applications. Thus, the presence of queue feedback would create adverse effects on the stability of the emerging limit cycles. In essence, the analytical results of RCP with two delays favor the design choice that uses feedback based only on rate mismatch. The theoretical analysis is validated with numerical computations and some packet level simulations as well.

Keywords: Rate Control Protocol, queue feedback, two delays, stability, Hopf bifurcation

*Correspondence to: A. Abuthahir, Department of Electrical Engineering, IIT Madras, Chennai 600036, India

Email addresses: ee12d207@ee.iitm.ac.in (Abuthahir), gaurav@ee.iitm.ac.in (Gaurav Raina)

1. Introduction

Internet congestion control has been an active area of research for several decades [25]. The Transmission Control Protocol (TCP) is the widely used transport layer protocol which control network congestion in the Internet. It has been shown that the performance of TCP is poor in the future high bandwidth delay network due to its use of implicit feedback and the standard Additive Increase Multiplicative Decrease (AIMD) control law [12]. This motivates the development of congestion control protocols that relies on more explicit feedback [4, 11, 17, 18, 19, 23, 31, 33]. Rate control protocol (RCP) is an explicit congestion control algorithm that received a lot of attention from the research community [1, 3, 2, 4, 13, 14, 15, 19, 20, 24, 28, 29, 35].

A key motivation for considering RCP, is that it continues to receive attention not only in the currently used host-centric (IP-based) networks, but also in the future data-centric networking architectures like Named Data Networking (NDN) [32]. In NDN, there is no IP address, and all data are named with unique names. Moreover, the data can be fetched from multiple sources via multiple paths which makes the implicit signaling mechanism unreliable in NDN [23]. Therefore, researchers focus on employing rate-based RCP-style algorithms in NDN [15, 19, 35]. For example, in [15] and [35], they combined RCP and the unique features of NDN to develop rate-based schemes for NDN congestion control. Similarly, RCP has attracted interest in wireless and satellite networks. In [3], RCP is extended with the support of an algorithm to accurately evaluate the capacity of wireless links. Simulation results in [28] reveal that RCP outperforms TCP in terms of throughput and queue size in the satellite networks. In [24], the feasibility of implementing RCP with flexible packet processing architectures has been demonstrated, especially in the data center networks. In this paper, our focus will be restricted to one particular design problem that arises in the study of feedback mechanism used by RCP. To expand further, RCP assigns a single fair rate for all the flows traversing the bottleneck link. These rates are computed using control equations at the routers, which in turn employ two forms of feedback: rate mismatch and the queue size. Simulation studies in [13] show that the queue size feedback in RCP, can cause the queue to be less accurately controlled. This conclusion was based on some initial simulations, and more work is needed before one could conclude that the queue size terms should be dropped from the protocol definition. In this paper, we focus on the proportionally fair variant of RCP which was introduced in [13]. The model considers single bottleneck network carrying flows with two different round-trip times.

An RCP router utilizes a field in the packet header to convey the fair share rate at which the flows can send data into the network. However, the feedback about the fair rate to end-systems is not instantaneous. Therefore, RCP works like a closed-loop control system with feedback delays. In general, the stability of a closed-loop system is sensitive to feedback delays, which normally necessitates a detailed stability analysis. Local stability analysis retains only the linear component and ignores all higher order terms of the non-linear system

before addressing the issue of stability. So, it looks appealing to have an analytical methodology which may allow us to capture the impact of some non-linear terms while performing a Taylor expansion of the non-linear system about its equilibrium. Local bifurcation theory is one such methodology [10]. A comprehensive understanding of local bifurcation phenomena may help yield insights into the role played by different forms of feedback in RCP. Moreover, any congestion control algorithm is not only to ensure local stability of the equilibrium, but also to make sure that any loss of stability, that may happen, results in *stable* limit cycles of small amplitude. We hasten to add that we are not interested in destabilizing our network, but wish to employ the tools offered by local instability analysis to gain some insight into the non-linear properties of both the design options, i.e., with and without queue size feedback. There is considerable interest in analyzing the stability and Hopf bifurcation of the congestion control algorithms [1, 5, 16, 21, 29, 34].

We now need to decide which parameter will be used to violate the stability condition and hence act as the bifurcation parameter. We motivate a non-dimensional exogenous parameter to induce instability. This has various advantages. We need not be concerned with the dimensions of the parameter, and as it is common for both the design choices we can compare the results fairly. By analyzing the roots of the transcendental characteristic equation, we first derive necessary and sufficient conditions for local asymptotic stability. This enables us to determine the stability region in the parameter space. It is then shown that, as the bifurcation parameter varies, the system where feedback is based on both rate mismatch and queue size, readily loses local stability through a Hopf bifurcation [10]. Then, we investigate the impact of queue feedback on the direction and stability of the emerging limit cycles. To that end, we conduct a detailed Hopf bifurcation analysis for both the design choices. The Appendix contains the necessary calculations to determine the type of Hopf bifurcation and the orbital stability of the bifurcating limit cycles, as local instability just sets in. The theoretical frameworks that we employ to analyze the nature of Hopf bifurcation are the Poincaré normal forms and the center manifold theorem. We establish that the RCP which uses only rate mismatch feedback would give rise to a super-critical Hopf bifurcation which leads to stable limit cycles of small amplitude. Whereas, in the presence of queue feedback, the system can exhibit a sub-critical Hopf bifurcation, for some parameter values. A sub-critical Hopf bifurcation is undesirable for real engineering systems as a small perturbation around the system equilibrium may give rise to either limit cycles with large amplitude, or unstable limit cycles [27]. The numerical analysis tool that we use to validate the theoretical insights is DDE-Biftool (a Matlab package for numerical bifurcation and stability analysis of delay differential equations) [6], [7].

In summary, the analytical insights of our study tend to favor the design choice where the feedback is based only on rate mismatch. Numerical computations and packet level simulations serve to corroborate the analysis.

The rest of the paper is organized as follows. In Section 2, we outline the non-linear fluid model of RCP. We analyze the local asymptotic stability of

RCP in Section 3. In Section 4, we conduct a local Hopf bifurcation analysis and highlight the impact of queue feedback on the nature of Hopf bifurcation. In Section 5, we conclude with a summary of our contributions, and offer avenues for further research. For ease of exposition, the Hopf bifurcation analysis is contained in an Appendix.

2. Models

The small buffer model of a proportionally fair RCP is governed by the following non-linear delay differential equation [13]

$$\frac{d}{dt}R_j(t) = \frac{aR_j(t)}{C_j\bar{T}_j(t)}\left(C_j - y_j(t) - b_jC_jp_j(y_j(t))\right), \quad (1)$$

where

$$y_j(t) = \sum_{r:j \in r} x_r(t - T_{rj})$$

is the aggregate load at link j summed over all the routes r passing through link j , $R_j(t)$ is the rate that RCP maintains for all flows passing through link j , $x_r(t)$ is the rate on route r , $p_j(y_j)$ is the mean queue size at link j when the arriving load is y_j , C_j is the capacity of link j , a and b_j are non-negative protocol parameters.

Here, T_j is the average round trip time of packets passing through link j given by

$$\bar{T}_j = \frac{\sum_{r:j \in r} x_r(t)T_r}{\sum_{r:j \in r} x_r(t)} \quad (2)$$

where,

$$T_r = T_{rj} + T_{jr} \quad (3)$$

is the sum of the propagation delay from source to link j and the return delay from link j to source. Here, we assume that the queuing delay is negligible as compared to the propagation delay, which conforms with our assumption of small buffers. The flow rate $x_r(t)$ is given by [13]

$$x_r(t) = \left(\sum_{j \in r} R_j(t - T_{jr})^{-1} \right)^{-1} \quad (4)$$

Now we will model the mean queue size term as follows. Suppose that workload arriving at resource of capacity C , over a time period τ is Gaussian with mean $y_j\tau$ and variance $y_j\tau\sigma_j^2$. The workload present at the queue reflects Brownian motion [9], with mean under its stationary distribution of

$$p(y_j) = \frac{y_j\sigma_j^2}{2(C - y_j)}. \quad (5)$$

The above relation is a simple approximation to mean queue size, where σ_j^2 represents the variability of traffic in the link at a packet level. We assume $\sigma_j = 1$, which corresponds to the Poisson arrival of packets of constant size.

For our analysis, we consider the network with single bottleneck link of capacity C , carrying two sets of RCP flows with different round trip times; say τ_1 and τ_2 . Then the model is given by

$$\frac{d}{dt}R(t) = \frac{aR(t)}{C\bar{T}(t)} \left(C - y(t) - bCp(y(t)) \right), \quad (6)$$

where

$$\begin{aligned} \bar{T} &= (\tau_1 + \tau_2)/2 \\ y(t) &= R(t - \tau_1) + R(t - \tau_2) \end{aligned}$$

To model the RCP without queue feedback, the parameter b is set to zero to exclude the queuing term from the RCP model. Then to aim for a particular target link utilisation, say a fraction γ of the actual link capacity, C is replaced with γC . Then the model of RCP without queue size feedback is given by

$$\frac{d}{dt}R(t) = \frac{aR(t)}{\gamma C\bar{T}(t)} \left(\gamma C - y(t) \right). \quad (7)$$

3. Local Stability Analysis

In this section, we derive conditions for local stability in terms of model parameters. We could induce instability by varying any of the system parameters. However, we prefer not to choose any of the system parameters, but introduce an exogenous non-dimensional parameter κ to push the system into the unstable regime.

3.1. With queue feedback

Let R^* denote the non-zero equilibrium of equation (6), then

$$R^* = \frac{C(4 + b - \sqrt{b^2 + 8b})}{8}. \quad (8)$$

Let $u(t) = R(t) - R^*$ be a perturbation about the equilibrium. Then linearising (6), about the equilibrium, gives

$$\frac{du(t)}{dt} = -\kappa\tilde{a}(u(t - \tau_1) + u(t - \tau_2)), \quad (9)$$

where

$$\tilde{a} = \frac{a}{(\tau_1 + \tau_2)} \left[1 + \frac{2R^*}{C} \right]. \quad (10)$$

Looking for exponential solutions, the characteristic equation of (9) is given by

$$\lambda + \kappa \tilde{a} (e^{-\lambda\tau_1} + e^{-\lambda\tau_2}) = 0, \quad (11)$$

where $\tilde{a}, \kappa, \tau_1, \tau_2 > 0$.

For the system to be stable, all the roots of the characteristic equation should lie in the left half of the complex plane. When the round-trip times are zero, we get $\lambda = -2\kappa\tilde{a} < 0$ and hence the system is asymptotically stable. However, when $\tau_1, \tau_2 > 0$ the roots may cross the imaginary axis for some values of the system parameters, and hence stability of the system cannot be guaranteed. Therefore, the condition for the crossover defines the bounds on the system parameters to maintain stability. To find the critical condition, where this crossover occurs, we substitute $\lambda = \pm i\omega$, $\omega > 0$ in (11). Equating the real and imaginary parts, we obtain

$$\kappa \tilde{a} (\cos(\omega\tau_1) + \cos(\omega\tau_2)) = 0, \quad (12)$$

$$\kappa \tilde{a} (\sin(\omega\tau_1) + \sin(\omega\tau_2)) = \omega. \quad (13)$$

Solving (12) and (13), we get

$$\omega(\tau_1 + \tau_2) = (2n + 1)\pi, \quad n = 0, 1, 2, \dots$$

We only treat the case $n = 0$, which gives $\omega_0 = \pi/(\tau_1 + \tau_2)$. We now use the following theorem, stated in [26], to get the stability condition.

Theorem 1. *The trivial solution of the scalar delay differential equation*

$$\dot{x}(t) + bx(t - \tau_1) + bx(t - \tau_2) = 0 \quad (14)$$

is exponentially asymptotically stable if and only if

$$0 < b < \frac{\pi}{2(\tau_1 + \tau_2) \cos\left(\frac{\pi(\tau_1 - \tau_2)}{2(\tau_1 + \tau_2)}\right)}. \quad (15)$$

Comparing (9) with (14), the necessary and sufficient condition for the stability of (9) can be written as

$$\kappa \tilde{a} (\tau_1 + \tau_2) \cos\left(\frac{\pi(\tau_1 - \tau_2)}{2(\tau_1 + \tau_2)}\right) < \frac{\pi}{2}. \quad (16)$$

Substituting the value of \tilde{a} in (16), we get

$$\kappa a \left[1 + \frac{2R^*}{C}\right] \cos\left(\frac{\pi(\tau_1 - \tau_2)}{2(\tau_1 + \tau_2)}\right) < \pi/2. \quad (17)$$

Since $\cos(\pi(\tau_1 - \tau_2)/2(\tau_1 + \tau_2)) \in (0, 1]$ for all values of $\tau_1, \tau_2 > 0$, we obtain the sufficient condition as

$$\kappa a \left[1 + \frac{2R^*}{C}\right] < \pi/2. \quad (18)$$

For $\kappa = 1$, using (8), we get

$$a \left[\frac{8 + b - \sqrt{b^2 + 8b}}{4} \right] < \pi/2. \quad (19)$$

See Fig. 1 which highlights the sufficient condition to ensure local stability for all values of $\tau_1, \tau_2 > 0$.

To show that the system loses local stability through Hopf bifurcation at a critical value of the bifurcation parameter, we need to satisfy the transversality condition of Hopf spectrum which has been outlined in the Appendix.

3.2. Without queue feedback

Proceeding as outlined in the previous sub-section, we get the necessary and sufficient condition for local stability of (7) as

$$\kappa a \cos \left(\frac{\pi(\tau_1 - \tau_2)}{2(\tau_1 + \tau_2)} \right) < \pi/2. \quad (20)$$

For $\kappa = 1$, we obtain the sufficient condition for stability as

$$a < \pi/2. \quad (21)$$

It is important to highlight that by excluding feedback based on queue size, we can increase the range of the parameter a for which the system is stable.

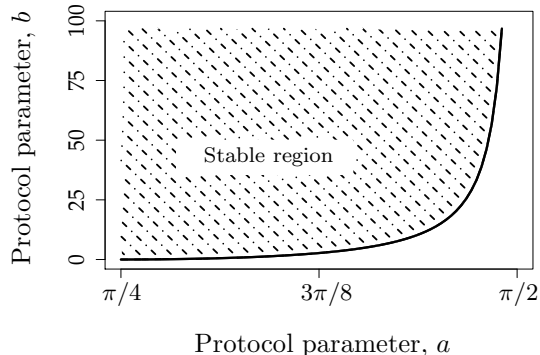


Figure 1: Stability chart for RCP with queue feedback, highlighting the sufficient condition to ensure local stability for all values of $\tau_1, \tau_2 > 0$.

We now resort to simulations to study the behaviour of RCP with and without queue feedback. The network being simulated has a single resource or bottleneck link, of capacity 100 packet per ms, and 100 sources creating Poisson traffic. Packet level simulations are done using discrete event simulator, which models the behaviour of the RCP network. Equation (8) serves as the relation between equilibrium utilisation and the parameter b when the queuing term is present in the RCP definition. for instance, to achieve utilisation of 75% of link

capacity, we need to set $b = 0.166$. To aim for the same utilisation in the case of RCP without queue feedback, we should set $b = 0$ and $\gamma = 0.75$. Packet-level traces shown in 2 illustrate that, in the presence of queue feedback, the system readily loses stability and leads to the emergence of limit cycles. These observations corroborate the results of our stability analysis which establish that the presence of queue size feedback is associated with a smaller choice of the protocol parameter a . So as far as the stability is concerned, the observations from simulations favor the design choice of having no queue size feedback in the RCP definition.

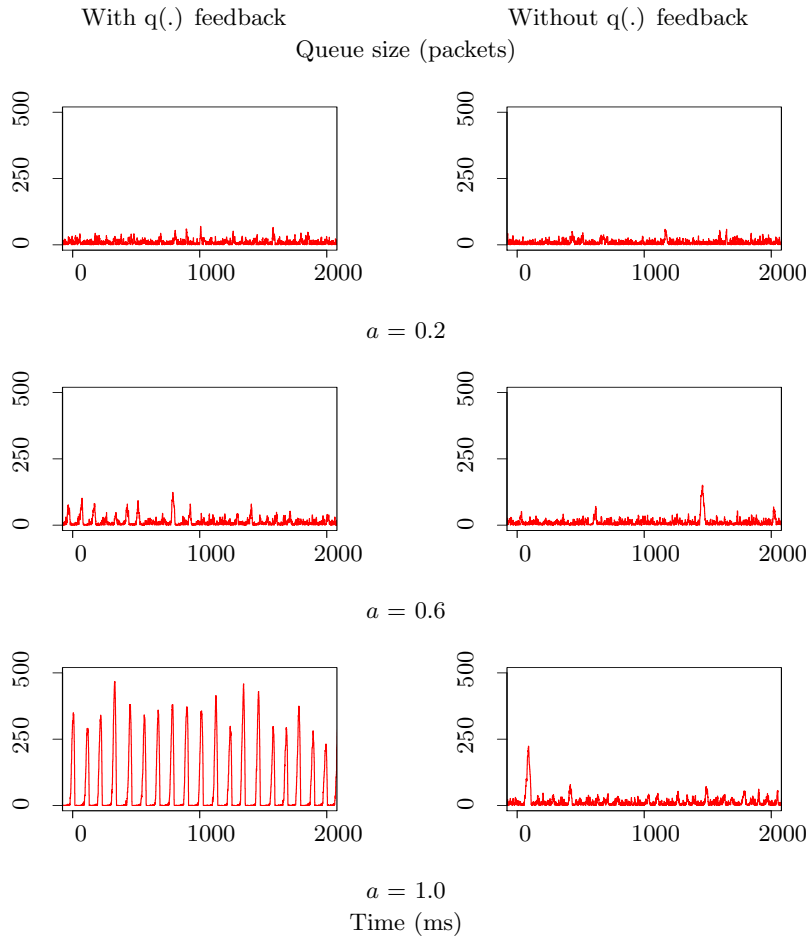


Figure 2: Traces from simulation of single bottleneck link with 100 RCP sources, $\tau_1 = 10$ ms, $\tau_2 = 50$ ms, $C = 100$ packets per ms, and target link utilisation of 95%.

4. Local Hopf Bifurcation Analysis

In stability analysis, we have shown that by excluding feedback based on queue size, we can increase the range of protocol parameter a , for which the stability is guaranteed. Also, we have established that the system loses local stability via a Hopf bifurcation and leads to the emergence of limit cycles. An important design objective of the system is not only to ensure the local stability for a wide range of parameters, but also to make sure that any loss of stability always result in stable limit cycles of small amplitude. So it is natural to study the characteristics of the bifurcating periodic solutions. To that end, we do a local Hopf bifurcation analysis.

The analytical framework employed to investigate the nature of the limit cycles are the Poincaré normal form and the center manifold theorem, which are outlined in the Appendix. The analysis relies on the linear, quadratic and cubic terms in the Taylor series expansion of (6) and (7), about equilibrium, which have been tabulated in Table 1. The coefficients not listed in the table do not exist.

4.1. Without queue feedback

In this section, we consider the small buffer model of RCP without queue feedback and perform the necessary calculations to determine the type of Hopf

Table 1: Linear, quadratic and cubic terms of a Taylor series expansion of (6) and (7) for RCP with small buffers. For brevity, the parameter τ_1, τ_2 represent the round-trip delays, ξ_x represents $f_x|_{(x^*, y^*, z^*)}$, ξ_y represents $f_y|_{(x^*, y^*, z^*)}$, ξ_z represents $f_z|_{(x^*, y^*, z^*)}$, ξ_{xx} represents $f_{xx}|_{(x^*, y^*, z^*)}$ and so on.

| | $b = 0$ | $b > 0$ |
|---------------------------------------|-----------------------------------|---|
| $\xi_y = \xi_z$ | $\frac{-a}{(\tau_1 + \tau_2)}$ | $\frac{-a(1 + (2R^*/C))}{(\tau_1 + \tau_2)}$ |
| $\xi_{xy} = \xi_{xz}$ | $\frac{-a}{R^*(\tau_1 + \tau_2)}$ | $\frac{-a(1 + (2R^*/C))}{R^*(\tau_1 + \tau_2)}$ |
| $2\xi_{yy} = \xi_{yz} = 2\xi_{zz}$ | 0 | $\frac{-2a}{(\tau_1 + \tau_2)\sqrt{bCR^*}}$ |
| $2\xi_{xyy} = \xi_{xyz} = 2\xi_{xzz}$ | 0 | $\frac{-2a}{(\tau_1 + \tau_2)R^*\sqrt{bCR^*}}$ |
| $\xi_{yyz} = \xi_{yzz}$ | 0 | $\frac{-3a}{(\tau_1 + \tau_2)bCR^*}$ |
| $\xi_{yyy} = \xi_{zzz}$ | 0 | $\frac{-a}{(\tau_1 + \tau_2)bCR^*}$ |

bifurcation and the asymptotic form of the bifurcation solutions as local instability just sets in. For now, we will only be concerned with the first Hopf bifurcation. As outlined in the appendix, the stability and direction of the bifurcating limit cycles can be determined from the sign of first Lyapunov coefficient (μ_2) and Floquet exponent (β_2), where

$$\mu_2 = \frac{-\text{Re}[c_1(0)]}{\alpha'(0)} \quad \beta_2 = 2 \text{Re}[c_1(0)].$$

Using the definitions outlined in the appendix and the values from Table 1, the expression for $\text{Re}[c_1(0)]$ has been calculated as

$$\text{sign} \left(\mathbf{Re}(c_1(0)) \right) = \text{sign} \left(\frac{2\pi \tilde{f}(\vartheta)}{(\gamma C)^2 (\tau_1 + \tau_2)} \right), \quad (22)$$

where

$$\begin{aligned} \vartheta &= \omega_0 \tau_1 = \frac{\pi \tau_1}{(\tau_1 + \tau_2)} \in (0, \pi), \\ \tilde{f}(\vartheta) &= -2\pi \sin^4(\vartheta) - \pi \sin^2(\vartheta) \cos^2(2\vartheta) \\ &\quad - 2 \cos(2\vartheta) \sin^3(\vartheta) \\ &\quad - \cos(2\vartheta) \sin^2(\vartheta) \cos(\vartheta) (\pi - 2\vartheta). \end{aligned}$$

From (22), we can say that the sign of $\text{Re}[c_1(0)]$ depends on $\tilde{f}(\vartheta)$. From Fig. 3, it is clear that the $\tilde{f}(\vartheta)$ is negative for all $\vartheta \in (0, \pi)$. Therefore $\mathbf{Re}(c_1(0))$ is negative for all $\vartheta \in (0, \pi)$. We have already shown that $\alpha'(0) > 0$ for all $\vartheta \in (0, \pi)$. Hence, we have $\mu_2 > 0$ and $\beta_2 < 0$ which enables us to conclude that the system undergoes a super-critical Hopf and the limit cycles are asymptotically orbitally stable.

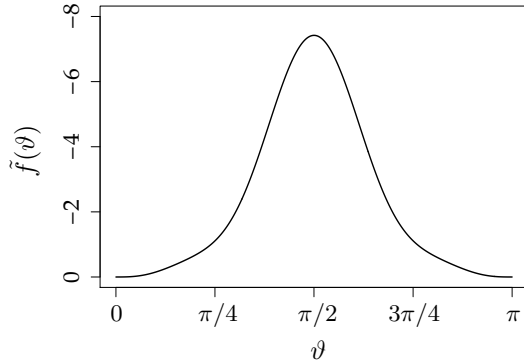


Figure 3: The plot of $\tilde{f}(\vartheta)$ as ϑ varies. As $\tilde{f}(\vartheta) < 0$ and hence $\mathbf{Re}(c_1(0)) < 0$, the Hopf bifurcation is super-critical and the limit cycles are orbitally stable.

4.2. With queue feedback

We now consider the RCP model which uses both rate mismatch and queue size feedback. Let us denote the equilibrium utilisation as

$$\rho^* = \frac{2R^*}{C} \quad (23)$$

Using the calculations outlined in the Appendix, we obtain the closed-form analytical expression for μ_2 as

$$\mu_2 = \frac{\mathbf{Re}(\tilde{g}(\vartheta, \rho^*)\bar{D})}{\mathbf{Re}(i(1 + \rho^*)\bar{D})} \quad (24)$$

where

$$\begin{aligned} \tilde{g}(\vartheta, \rho^*) = & \frac{\sin(\vartheta)}{\rho^*(1 - \rho^*)} \left(2i \sin(\vartheta) - \frac{2 \cos(2\vartheta) + i \sin(\vartheta)}{\cos(2\vartheta) + 2i \sin(\vartheta)} \right) \\ & + \frac{(1 + \rho^*)(-\sin(\vartheta) + i \cos(2\vartheta))}{(\rho^*)^2(\cos(2\vartheta) + 2i \sin(\vartheta))} \\ & + \frac{2 \sin^2(\vartheta)(-4 \sin(\vartheta) + 3i \cos(2\vartheta))}{(1 - \rho^*)^2(1 + \rho^*)(\cos(2\vartheta) + 2i \sin(\vartheta))} \\ & - \frac{3i(3 \sin(\vartheta) - \sin(3\vartheta))}{4(1 - \rho^*)^2 \sin(\vartheta)} \end{aligned} \quad (25)$$

It is to be noted that the protocol parameter a has no effect on the nature of the Hopf bifurcation. The criticality of the Hopf bifurcation and the oscillation amplitude depends on the value of μ_2 . In this case, we go for numerical examples to study the nature of Hopf bifurcation.

Numerical Example 1: Let us consider $b = 0.022$ which corresponds to equilibrium utilisation of $\rho^* = 0.9$. The values of μ_2 computed using (25) for all $\vartheta \in (0, \pi)$ has been plotted in Fig. 4. From Fig. 4, we can observe that both super-critical and sub-critical Hopf occurs, and the criticality varies with ϑ which is a function of τ_1 and τ_2 .

Numerical Example 2: Now we assume $\tau_2 = 2\tau_1$ which corresponds to $\vartheta = \pi/3$, and vary the equilibrium utilisation to analyze its impact on the criticality of the Hopf bifurcation. Fig. 5 shows the computed values of μ_2 for $\rho^* \in (0, 1)$. As the equilibrium utilisation increases, the criticality of the bifurcation changes from super-critical to sub-critical and so there is the potential for large amplitude limit cycles which is undesirable.

To summarise, the results of the local Hopf bifurcation analysis enables us to say that the RCP without queue feedback undergoes super-critical Hopf bifurcation and leads to orbitally stable limit cycles. Whereas, we observed sub-critical Hopf bifurcation for some parameter values if the queue size feedback is incorporated into the RCP model. The super-critical case is highly desirable from a performance viewpoint than the sub-critical one, since the sub-critical Hopf

bifurcation results in sharp loss of system stability. Therefore, the removal of queue size feedback would be the most appropriate design choice for RCP.

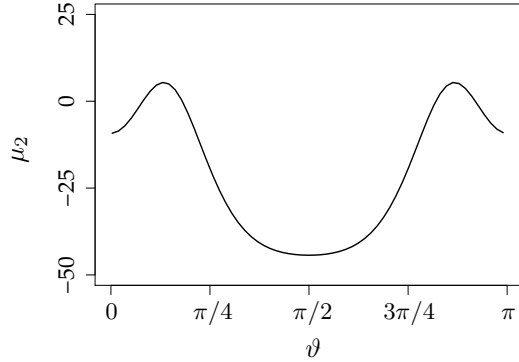


Figure 4: Effect of ϑ on the criticality of the Hopf bifurcation: sub-critical if $\mu_2 < 0$ and super-critical if $\mu_2 > 0$.

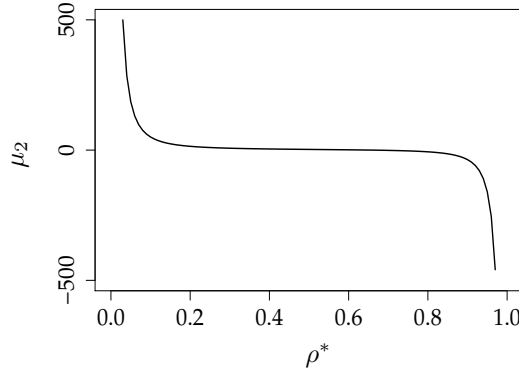


Figure 5: The plot of μ_2 as equilibrium utilization (ρ^*) varies. For low ρ^* , $\mu_2 > 0$ and hence the Hopf bifurcation is super-critical. For high ρ^* , $\mu_2 < 0$ which implies that the Hopf bifurcation is sub-critical.

4.3. Numerical computations

In a scalar non-linear equation with two discrete delays, both the delays play an important role in determining the type of the Hopf bifurcation. As we have just witnessed that even with the same non-linear term, by simply changing the values of the delay, we can change the type of the Hopf bifurcation.

We now validate the analytical results using some numerical examples.

4.3.1. When round-trip times vary

Numerical Example 1 (Super-critical): Let us consider the RCP system with $C = 100$, $\tau_1 = 10$ and $\tau_2 = 70$ which corresponds to $\vartheta = \pi/8$. We set $b = 0.022$ which corresponds to equilibrium utilization of 90% of link capacity i.e., $\rho^* = 0.9$. For these values, using (17), we obtain $a = 2.16$, for $\kappa_c = 1$. From Figure 4, we can observe that the value of μ_2 is positive, implying that the system undergoes a super-critical Hopf bifurcation. The bifurcation diagram drawn using the Matlab package DDE-Biftool [6, 7] is shown in Figure 6. As expected, it shows that the system loses local stability via a super-critical Hopf bifurcation, as the bifurcation parameter crosses the critical threshold ($\kappa_c = 1$). To validate this, numerical simulations obtained using XPPAUT [8] are shown in Figure 7. For $\kappa = 0.95$, the system converges to the equilibrium rate, $R^* = 45$ (see Figure 7(a)). Whereas, for $\kappa = 1.05 > \kappa_c$ i.e. after the bifurcation, the system leads to the emergence of stable limit cycles.

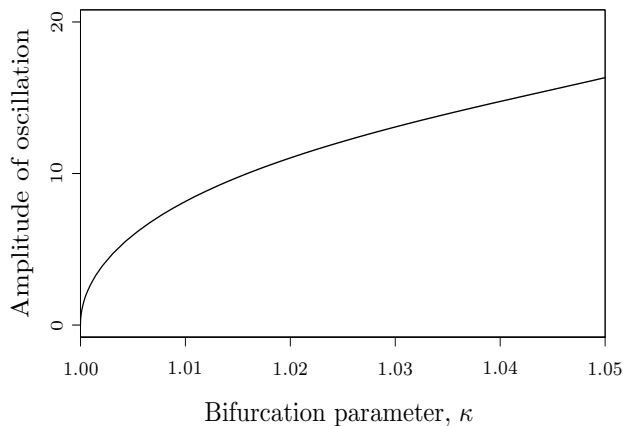


Figure 6: Bifurcation diagram highlighting that the system undergoes a super-critical Hopf bifurcation at $\kappa = 1$. The parameter values used are $a = 2.16$, $b = 0.022$, $C = 100$, $\tau_1 = 10$ and $\tau_2 = 70$ ($\vartheta = \pi/8$).

Numerical Example 2 (Sub-critical): Consider $a = 0.87$, $b = 0.022$, $C = 100$, $\tau_1 = 10$ and $\tau_2 = 15$ ($\vartheta = 2\pi/5$). The system undergoes a Hopf bifurcation at $\kappa = 1$. For these values, from Figure 4, we get $\mu_2 < 0$, implying that the system undergoes a sub-critical Hopf. We can also observe from Figure 8 that there exists no stable limit cycle in the neighborhood, as the bifurcation parameter is varied beyond the critical threshold. Hence the Hopf bifurcation is sub-critical and the bifurcating limit cycles are unstable. To illustrate the occurrence of a sub-critical Hopf, we present some numerical simulations in Figure 9. For $\kappa = 0.95$, the system converges to the stable equilibrium, $R^* = 45$ (see Figure 9(a)). Whereas, after the bifurcation i.e. for $\kappa > \kappa_c$, the previously stable fixed point now becomes unstable and also the solution would eventually jump to infinity (Figure 9(b)).

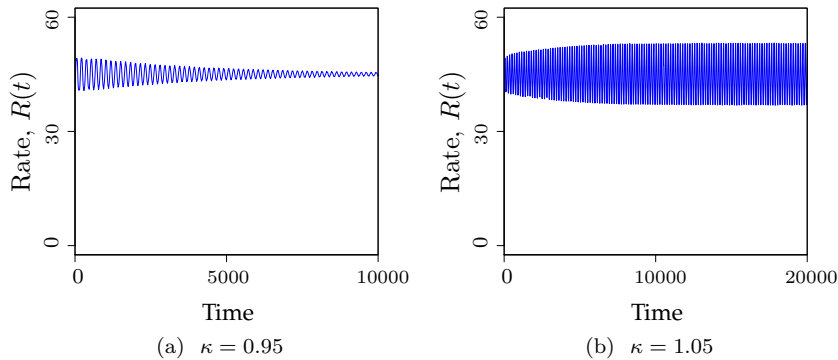


Figure 7: Numerical simulations illustrating that the system exhibits a super-critical Hopf bifurcation, as κ increases beyond the critical value. Time series are shown for the cases $\kappa < 1$ and $\kappa > 1$. The parameter values chosen are $a = 2.16$, $b = 0.022$, $C = 100$, $\tau_1 = 10$, $\tau_2 = 70$.

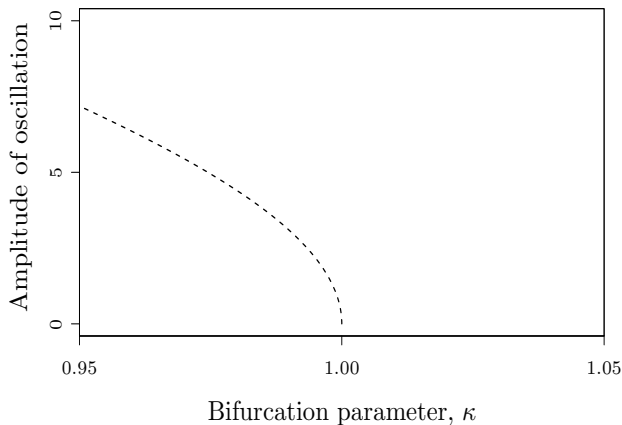


Figure 8: Bifurcation diagram showing the existence of a sub-critical Hopf for $a = 0.87$, $b = 0.022$, $C = 100$, $\tau_1 = 10$ and $\tau_2 = 15$ ($\vartheta = 2\pi/5$).

4.3.2. When target link utilization varies

Numerical Example 1 (Super-critical): Let us consider the RCP system with $C = 100$, $\tau_1 = 10$ and $\tau_2 = 20$ which corresponds to $\vartheta = \pi/3$. We set $b = 0.736$ which corresponds to equilibrium utilization of 55% of link capacity i.e., $\rho^* = 0.55$. For these values, using (17), we obtain $a = 1.17$, for $\kappa_c = 1$. From Figure 5, we can observe that $\mu_2 > 0$ for $\rho^* = 0.55$, implying that the system undergoes a super-critical Hopf bifurcation. The bifurcation diagram drawn using the Matlab package DDE-Biftool is shown in Figure 10. As expected, it shows that the system loses local stability via a super-critical Hopf bifurcation, as the bifurcation parameter crosses the critical threshold ($\kappa_c = 1$). To validate

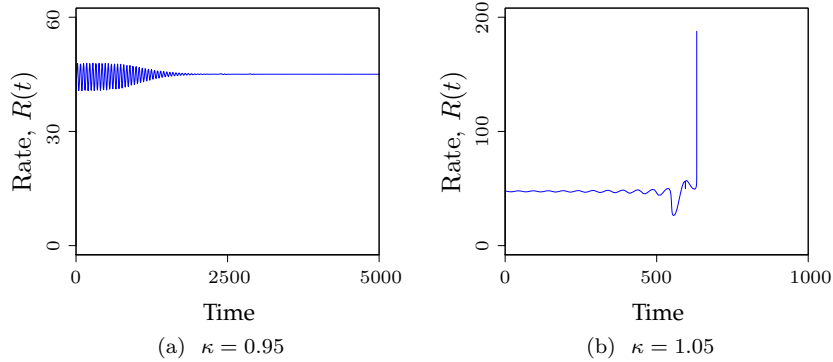


Figure 9: Numerical simulations highlighting that the system undergoes a sub-critical Hopf for the parameter values $\kappa_c = 1$, $a = 0.827$, $\tau = 100$, $C = 10$ and $b = 0.022$.

this, numerical simulations obtained using XPPAUT are shown in Figure 11. For $\kappa = 0.95$, the system converges to the equilibrium rate, $R^* = 27.5$ (see Figure 11(a)). Whereas, for $\kappa = 1.05 > \kappa_c$ i.e. after the bifurcation, the system leads to the emergence of stable limit cycles.

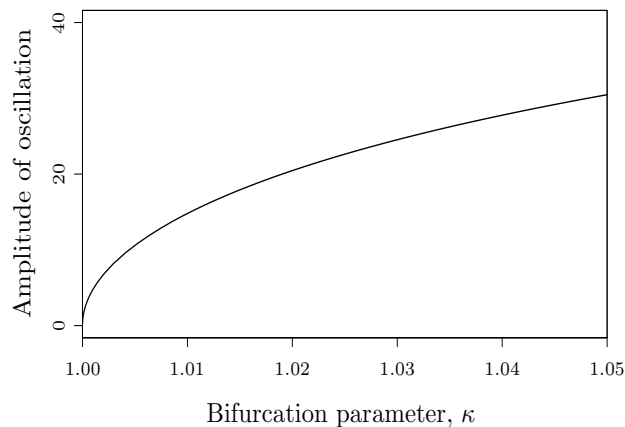


Figure 10: Bifurcation diagram highlighting that the system undergoes a super-critical Hopf bifurcation at $\kappa = 1$. The parameter values used are $a = 1.17$, $b = 0.736$, $C = 100$, $\tau_1 = 10$ and $\tau_2 = 20$ ($\vartheta = \pi/3$).

Numerical Example 2 (Sub-critical): Consider $a = 0.95$, $b = 0.022$ ($\rho^* = 0.9$), $C = 100$, $\tau_1 = 10$ and $\tau_2 = 20$. The system undergoes a Hopf bifurcation at $\kappa = 1$. For these values, from Figure 5, we get $\mu_2 < 0$, implying that the system undergoes a sub-critical Hopf. We can also observe from Figure 12 that there

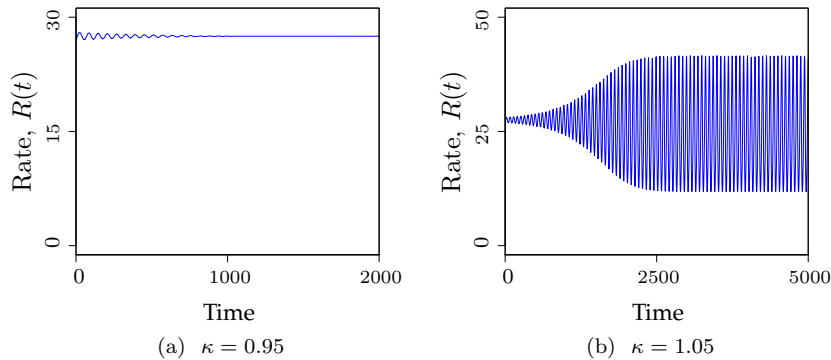


Figure 11: Numerical simulations illustrating that the system exhibits a super-critical Hopf bifurcation, as κ increases beyond the critical value. Time series are shown for the cases $\kappa < 1$ and $\kappa > 1$. The parameter values chosen are $a = 1.17$, $b = 0.736$, $C = 100$, $\tau_1 = 10$, $\tau_2 = 20$.

exists no stable limit cycle in the neighborhood, as the bifurcation parameter is varied beyond the critical threshold. Hence, the Hopf bifurcation is sub-critical and the bifurcating limit cycles are unstable. To illustrate the occurrence of

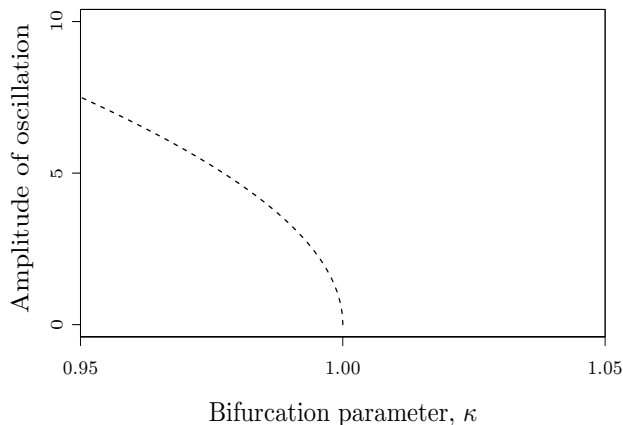


Figure 12: Bifurcation diagram showing the existence of a sub-critical Hopf for $a = 0.95$, $b = 0.022$, $C = 100$, $\tau_1 = 10$ and $\tau_2 = 20$.

a sub-critical Hopf, we present some numerical simulations in Figure 13. For $\kappa = 0.95$, the system converges to the stable equilibrium, $R^* = 45$ (see Figure 13(a)). Whereas, after the bifurcation i.e. for $\kappa > \kappa_c$, the previously stable fixed point now becomes unstable and also the solution would eventually jump to infinity (Figure 13(b)).

In summary, the results of theoretical and numerical analysis reveal that the

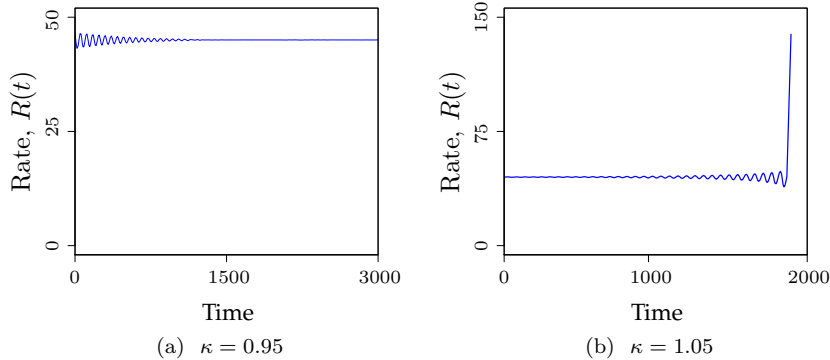


Figure 13: Numerical simulations highlighting that the system undergoes a sub-critical Hopf for the parameter values $\kappa_c = 1$, $a = 0.95$, $\tau = 100$, $C = 10$ and $b = 0.022$.

RCP which uses both rate mismatch and queue size feedback, can undergo a sub-critical Hopf bifurcation, which is undesirable for engineering applications. In fact, in the context of congestion control algorithms, the possibility of occurrence of a sub-critical Hopf has not been extensively studied so far. The insights from Hopf bifurcation analysis could guide design considerations such that any loss of local stability only occurs via the emergence of small amplitude stable limit cycles. In other words, the nature of Hopf bifurcation and the stability of the bifurcating limit cycles should also be considered while designing congestion control protocols.

4.4. Packet-level simulations

We now validate some of the theoretical insights by investigating if the packet-level simulations of the underlying system exhibits the qualitative properties predicted through the Hopf bifurcation analysis of the fluid model. The packet-level simulations are done using a discrete event RCP simulator (for more details, refer to [13]). The simulated network has a single bottleneck link setup that considers Capacity, $C = 1$ Giga bits per sec (Gbps) and number of sources = 100.

Simulation traces in Figure 14 show the evolution of queue size and flow rate for the cases with and without queue size feedback. We choose $\tau_1 = 100$ ms for half of the flows and $\tau_2 = 150$ ms for the remaining 50 flows. Here, we set $b = 0.005$ which corresponds to equilibrium utilization of 95% of link capacity. For RCP without queue size feedback, we set $\gamma = 0.95$ to achieve the same target link utilization. We can observe that the RCP which uses both rate mismatch and queue feedback exhibits large amplitude limit cycles (due to the occurrence of a sub-critical Hopf). Whereas, in the absence of queue feedback, the system undergoes a super-critical Hopf bifurcation, and leads to the emergence of small amplitude limit cycles.

From the simulation traces shown in Figure 15, we can observe that, in the presence of queue feedback, the type of Hopf bifurcation can be varied by changing the values of τ_1 and τ_2 .

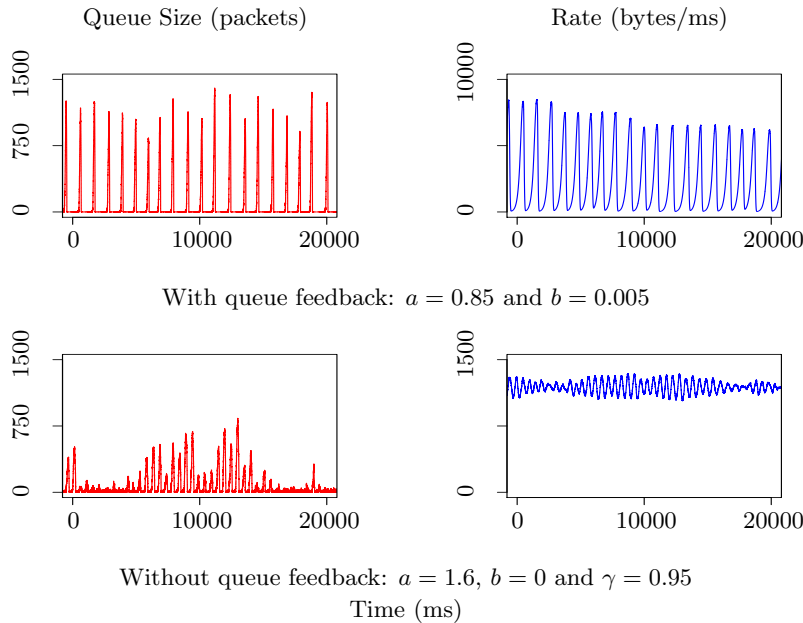


Figure 14: Simulation traces highlighting that the system which includes queue feedback exhibits limit cycles with amplitude much larger than that of RCP which uses only rate mismatch feedback. The parameter values used are i) with queue feedback: $a = 0.85$, $b = 0.005$ and ii) without queue feedback: $a = 1.6$, $\gamma = 0.95$. We consider round-trip times of $\tau_1 = 100$ ms and $\tau_2 = 150$ ms.

5. Contributions

RCP estimates the fair rate of flows using feedback based on rate mismatch and queue size. An open design question in RCP is whether it is advantageous to include queue size feedback, given that the protocol already includes feedback based on rate mismatch. To address this question, we analyzed stability and Hopf bifurcation properties for both the design options, i.e., with and without queue size feedback. In this paper, we considered the RCP model that assumes single bottleneck link carrying flows with two different round-rip times. In the local stability analysis, we showed that in the presence of queue feedback, the system readily loses its stability via a Hopf bifurcation, as the bifurcation parameter varies. For our analysis, a dimensionless exogenous parameter was used as the bifurcation parameter. Then, we proceeded to analyze the dynamics of both the design choices for stability are just violated. From a bifurcation theoretic perspective we would like our algorithms to always produce

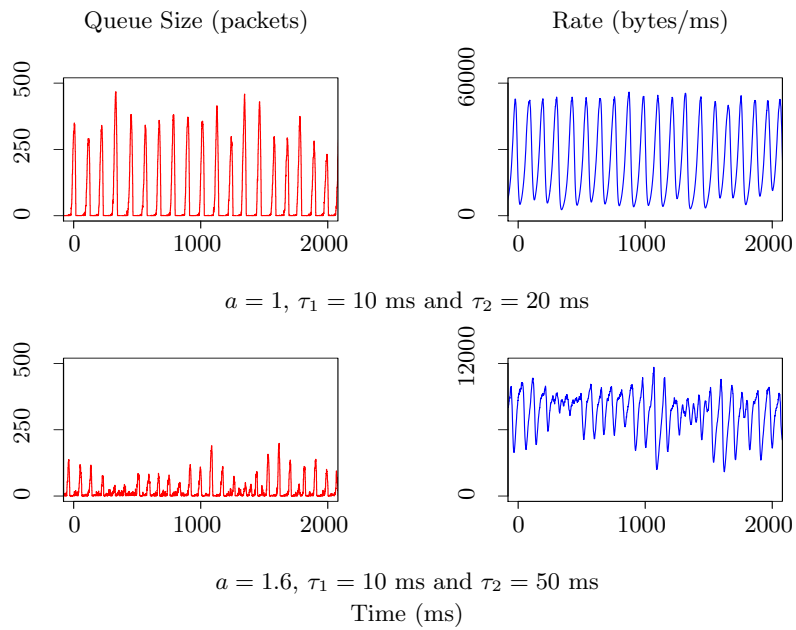


Figure 15: Simulation traces highlighting that the system which includes queue feedback exhibits both super-critical and sub-critical Hopf, depending on the values of RTTs. We set $b = 0.005$ which corresponds to the target utilization of 95% of link capacity.

stable limit cycles of small amplitude. We analyzed the type of Hopf bifurcation and the orbital stability of the bifurcating limit cycles. We highlighted that the presence of queue feedback in RCP results in a sub-critical Hopf bifurcation, for some parameter values. A sub-critical Hopf leads to either large amplitude limit cycles or unstable limit cycles, and hence its occurrence should be avoided. Whereas, in the absence of queue feedback, the Hopf bifurcation is always super-critical and leads to the emergence of stable limit cycles of small amplitude. Hence, it is advisable to go with the design choice that uses only rate mismatch feedback. We complemented the analysis with bifurcation diagrams, numerical computations, and packet-level simulations.

Naturally, the work should also extend to consider the cases with multi bottleneck link. It is also worth investigating the global stability of RCP both in the presence and absence of queue feedback.

Appendix A. Hopf Bifurcation Analysis

Appendix A.1. Existence of Hopf bifurcation

Stability analysis highlights that the RCP loses stability at a critical value of bifurcation parameter κ ; $\kappa=\kappa_c$. Therefore, we obtain the critical value of the bifurcation parameter, at which the system loses local stability, as

$$\kappa_c = \frac{\pi}{2\tilde{a}(\tau_1 + \tau_2) \cos\left(\frac{\omega_0(\tau_1 - \tau_2)}{2}\right)}. \quad (\text{A.1})$$

To show that the system undergoes a Hopf bifurcation at κ_c , we need to satisfy the following transversality condition of the Hopf spectrum [10]

$$\mathbf{Re}\left(\frac{d\lambda}{d\kappa}\right)_{\kappa=\kappa_c} \neq 0.$$

Now we consider the linear autonomous delay equation of the system whose corresponding characteristic equation is given by

$$\lambda + \kappa\tilde{a}(e^{-\lambda\tau_1} + e^{-\lambda\tau_2}) = 0. \quad (\text{A.2})$$

Differentiating the above equation with respect to κ , we get

$$\left.\frac{d\lambda}{d\kappa}\right|_{\kappa=\kappa_c} = \left.\frac{-\tilde{a}(e^{-\lambda\tau_1} + e^{-\lambda\tau_2})}{(1 - \kappa\tilde{a}(\tau_1 e^{-\lambda\tau_1} + \tau_2 e^{-\lambda\tau_2}))}\right|_{\kappa=\kappa_c}.$$

Substituting the values, we obtain

$$\mathbf{Re}\left(\frac{d\lambda}{d\kappa}\right)_{\kappa=\kappa_c} = \frac{\pi\tilde{a}\sin(\omega_0\tau_1)}{A^2 + B^2} > 0,$$

where

$$\begin{aligned}\omega_0 &= \pi/(\tau_1 + \tau_2) \\ A &= 1 - \frac{\omega_0 \cos(\omega_0 \tau_1)(\tau_1 - \tau_2)}{2 \sin(\omega_0 \tau_1)} \\ B &= \pi/2.\end{aligned}$$

Now we have shown the existence of Hopf bifurcation at the edge of the stable regime. It is important to note that the result holds true for both the cases i.e. with, and without queue feedback, as $\tilde{a} > 0$ for both.

Appendix A.2. Type and stability of Hopf bifurcation

We have shown that the system exhibits Hopf type bifurcation in both the cases i.e. with, and without queue feedback. However a comprehensive understanding of the stability and amplitudes of the emerging limit cycles would certainly help to address the question of whether the queue feedback is useful, or not.

Here, we outline the necessary calculations to determine the type of Hopf bifurcation and the asymptotic form of the bifurcation solutions as local instability just sets in. For now, we will only be concerned with the first Hopf bifurcation. The framework employed to address the stability of the limit cycles is the Poincaré normal form, and the center manifold theorem.

Consider the following nonlinear delay differential equation:

$$\frac{d}{dt}x(t) = \kappa f(x(t), x(t - \tau_1), x(t - \tau_2)), \quad (\text{A.3})$$

where f has a unique equilibrium denoted by x^* and $\tau_1, \tau_2 > 0$. Define $u(t) = x(t) - x^*$, and take a Taylor expansion for (A.3) including the linear, quadratic and cubic terms to obtain

$$\begin{aligned}\frac{d}{dt}u(t) &= \kappa(\xi_y u(t - \tau_1) + \xi_z u(t - \tau_2) + \xi_{xy} u(t)u(t - \tau_1) \\ &+ \xi_{xz} u(t)u(t - \tau_2) + \xi_{yy} u^2(t - \tau_1) \\ &+ \xi_{yz} u(t - \tau_1)u(t - \tau_2) + \xi_{zz} u^2(t - \tau_2) \\ &+ \xi_{xyy} u(t)u^2(t - \tau_1) + \xi_{xzz} u(t)u^2(t - \tau_2) \\ &+ \xi_{xyz} u(t)u(t - \tau_1)u(t - \tau_2) + \xi_{yyy} u^3(t - \tau_1) \\ &+ \xi_{yyz} u^2(t - \tau_1)u(t - \tau_2) + \xi_{zzz} u^3(t - \tau_2) \\ &+ \xi_{yzz} u(t - \tau_1)u^2(t - \tau_2) + \mathcal{O}(u^4))\end{aligned} \quad (\text{A.4})$$

where, letting f^* denote evaluation of f at (x^*, y^*, z^*)

$$\begin{aligned}\xi_i &= f_i^*, & \xi_{ii} &= \frac{1}{2}f_{ii}^*, & \xi_{iii} &= \frac{1}{6}f_{iii}^* \quad \forall i \in \{x, y, z\} \\ \xi_{xy} &= f_{xy}^*, & \xi_{xz} &= f_{xz}^*, & \xi_{yz} &= f_{yz}^*, & \xi_{xxy} &= \frac{1}{2}f_{xxy}^* \\ \xi_{xxz} &= \frac{1}{2}f_{xxz}^*, & \xi_{xyy} &= \frac{1}{2}f_{xyy}^*, & \xi_{xzz} &= \frac{1}{2}f_{xzz}^* \\ \xi_{xyz} &= f_{xyz}^*, & \xi_{yyz} &= \frac{1}{2}f_{yyz}^*, & \xi_{yzz} &= \frac{1}{2}f_{yzz}^*.\end{aligned}$$

The calculations that follow will enable us to address questions about the form of the bifurcating solutions, as the system transits from stability to instability via a Hopf bifurcation. For this we have to take higher order terms, i.e., the quadratic and cubic of (A.4) into consideration. Following the work of [22], we now perform the requisite calculations.

Consider the following autonomous delay-differential system

$$\frac{d}{dt}u(t) = \mathcal{L}_\mu u_t + \mathcal{F}(u_t, \mu), \quad (\text{A.5})$$

where $t > 0$, $\mu \in \mathbb{R}$, $\tau = \max(\tau_1, \tau_2) > 0$,

$$u_t(\theta) = u(t + \theta), \quad u : [-\tau, 0] \rightarrow \mathbb{R}, \quad \theta \in [-\tau, 0].$$

\mathcal{L}_μ is a one-parameter family of continuous linear operators defined as $\mathcal{L}_\mu : C[-\tau, 0] \rightarrow \mathbb{R}$. The operator $\mathcal{F}(u_t, \mu) : C[-\tau, 0] \rightarrow \mathbb{R}$ contains the nonlinear terms. Further, assume that $\mathcal{F}(u_t, \mu)$ is analytic and that \mathcal{F} and \mathcal{L}_μ depend analytically on the bifurcation parameter. Note that (A.4) is a type of the form (A.5). The objective now is to rewrite (A.5) as follow

$$\frac{d}{dt}u_t = \mathcal{A}(\mu)u_t + \mathcal{R}u_t \quad (\text{A.6})$$

which has u_t rather than both u and u_t . By the Riesz representation theorem, there exists a matrix-valued function $\eta(\cdot, \mu) : [-\tau, 0] \rightarrow \mathbb{R}^{n^2}$, with variation of each component of η is bounded and for all $\phi \in C[-\tau, 0]$

$$\mathcal{L}_\mu \phi = \int_{-\tau}^0 d\eta(\theta, \mu)\phi(\theta),$$

where $d\eta(\theta, \mu) = \kappa(\xi_y\delta(\theta + \tau_1) + \xi_z\delta(\theta + \tau_2))d\theta$ and $\delta(\theta)$ is the Dirac delta function.

Now we define

$$\mathcal{A}(\mu)\phi(\theta) = \begin{cases} \frac{d\phi(\theta)}{d\theta}, & \theta \in [-\tau, 0), \\ \int_{-\tau}^0 d\eta(s, \mu)\phi(s), & \theta = 0, \end{cases} \quad (\text{A.7})$$

and

$$\mathcal{R}\phi(\theta) = \begin{cases} 0, & \theta \in [-\tau, 0), \\ \mathcal{F}(\phi, \mu), & \theta = 0. \end{cases}$$

Now the system (A.5) becomes equivalent to (A.6) as required.

Let $q(\theta)$ be the eigenfunction for $\mathcal{A}(0)$ corresponding to $\lambda(0)$, namely

$$\mathcal{A}(0)q(\theta) = i\omega_0 q(\theta).$$

Now we define an adjoint operator $\mathcal{A}^*(0)$ as

$$\mathcal{A}^*(0)\alpha(s) = \begin{cases} -\frac{d\alpha(s)}{ds}, & s \in (0, \tau], \\ \int_{-\tau}^0 d\eta^T(t, 0)\alpha(-t), & s = 0. \end{cases}$$

Note that, the domains of \mathcal{A} and \mathcal{A}^* are $C^1[-\tau, 0]$ and $C^1[0, \tau]$ respectively. As

$$\mathcal{A}q(\theta) = \lambda(0)q(\theta)$$

$\bar{\lambda}(0)$ is an eigenvalue for \mathcal{A}^* , and

$$\mathcal{A}^*q^* = -i\omega_0 q^*$$

for some nonzero vector q^* . For $\phi \in C[-\tau, 0]$ and $\psi \in C[0, \tau]$, define a bilinear inner product

$$\langle \psi, \phi \rangle = \bar{\psi}(0) \cdot \phi(0) - \int_{\theta=-\tau}^0 \int_{\varsigma=0}^{\theta} \bar{\psi}^T(\varsigma - \theta) d\eta(\theta) \phi(\varsigma) d\varsigma. \quad (\text{A.8})$$

Then, $\langle \psi, \mathcal{A}\phi \rangle = \langle \mathcal{A}^*\psi, \phi \rangle$ for $\phi \in \text{Dom}(\mathcal{A})$, $\psi \in \text{Dom}(\mathcal{A}^*)$. Let $q(\theta) = e^{i\omega_0\theta}$ and $q^*(s) = D e^{i\omega_0 s}$ be the eigenvectors for \mathcal{A} and \mathcal{A}^* corresponding to the eigenvalues $+i\omega_0$ and $-i\omega_0$.

Value of D can be evaluated using (A.8) and the relation $\langle q^*, q \rangle = 1$ as

$$\begin{aligned} \langle q^*, q \rangle &= \bar{D} - \bar{D}\kappa \int_{\theta=-\tau}^0 \theta e^{i\omega_0\theta} (\xi_y \delta(\theta + \tau_1) \\ &\quad + \xi_z \delta(\theta + \tau_2)) d\theta \\ \Rightarrow 1 &= \bar{D} + \bar{D}\kappa (\tau_1 \xi_y e^{-i\omega_0\tau_1} + \tau_2 \xi_z e^{-i\omega_0\tau_2}) \\ \Rightarrow D &= \frac{1}{1 + \kappa\tau_1 \xi_y e^{i\omega_0\tau_1} + \kappa\tau_2 \xi_z e^{i\omega_0\tau_2}}. \end{aligned}$$

Again, using (A.8) we show that $\langle q^*, \bar{q} \rangle = 0$ as

$$\begin{aligned} \langle q^*, \bar{q} \rangle &= \bar{D} + \frac{\bar{D}\kappa}{2i\omega_0} \int_{\theta=-\tau}^0 (e^{-i\omega_0\theta} - e^{i\omega_0\theta}) \\ &\quad \times (\xi_y \delta(\theta + \tau_1) + \xi_z \delta(\theta + \tau_2)) d\theta, \\ &= \bar{D} + \frac{\bar{D}\kappa}{2i\omega_0} (\xi_y (e^{i\omega_0\tau_1} - e^{-i\omega_0\tau_1}) \\ &\quad + \xi_z (e^{i\omega_0\tau_2} - e^{-i\omega_0\tau_2})), \\ &= 0. \end{aligned}$$

Now we define

$$\begin{aligned} z(t) &= \langle q^* \cdot u_t \rangle \text{ and} \\ w(t, \theta) &= u_t(\theta) - 2\text{Re}\{z(t)q(\theta)\}. \end{aligned} \quad (\text{A.9})$$

Then, on the centre manifold C_0 ,
 $w(t, \theta) = w(z(t), \bar{z}(t), \theta)$ where

$$w(z, \bar{z}, \theta) = w_{20}(\theta) \frac{z^2}{2} + w_{11}(\theta) z\bar{z} + w_{02}(\theta) \frac{\bar{z}^2}{2} + \dots \quad (\text{A.10})$$

In effect, z and \bar{z} are local coordinates for manifold in C in the directions of q^* and \bar{q}^* , respectively. The existence of the center manifold C_0 enables us to reduce (A.6) to an ordinary differential equation for a single complex variable on C_0 . At $\mu = 0$, we have

$$\begin{aligned} z'(t) &= \langle q^*, \mathcal{A}y_t + \mathcal{R}u_t \rangle \\ &= i\omega_0 z(t) + \bar{q}^*(0) \cdot \mathcal{F}(w(z, \bar{z}, \theta) + 2\text{Re}\{z(t)q(\theta)\}) \\ &= i\omega_0 z(t) + \bar{q}^*(0) \cdot \mathcal{F}_0(z, \bar{z}) \end{aligned} \quad (\text{A.11})$$

which can be written as

$$z'(t) = i\omega_0 z(t) + g(z, \bar{z}). \quad (\text{A.12})$$

Now expanding the function $g(z, \bar{z})$ in powers of z and \bar{z} we get

$$\begin{aligned} g(z, \bar{z}) &= \bar{q}^*(0) \cdot \mathcal{F}_0(z, \bar{z}) \\ &= g_{20} \frac{z^2}{2} + g_{11} z\bar{z} + g_{02} \frac{\bar{z}^2}{2} + g_{21} \frac{z^2 \bar{z}}{2} + \dots \end{aligned}$$

Following [10], we write

$$w' = u'_t - z'q - \bar{z}'\bar{q}. \quad (\text{A.13})$$

From (A.6) and (A.12) we get

$$w' = \begin{cases} Aw - 2\text{Re}\{\bar{q}^*(0) \cdot \mathcal{F}_0 q(\theta)\}, & \theta \in [-\tau_2, 0) \\ Aw - 2\text{Re}\{\bar{q}^*(0) \cdot \mathcal{F}_0 q(0)\} + \mathcal{F}_0, & \theta = 0 \end{cases}$$

which can be written as

$$w' = Aw + H(z, \bar{z}, \theta), \quad (\text{A.14})$$

using (A.12), where

$$H(z, \bar{z}, \theta) = H_{20}(\theta) \frac{z^2}{2} + H_{11}(\theta) z\bar{z} + H_{02}(\theta) \frac{\bar{z}^2}{2} + \dots \quad (\text{A.15})$$

Now, on the centre manifold C_0 , near the origin

$$w' = w_z z' + w_{\bar{z}} \bar{z}'.$$

Use (A.10) and (A.12) to replace w_z, z' and equating this with (A.14), we get

$$(2i\omega_0 - A)w_{20}(\theta) = H_{20}(\theta) \quad (\text{A.16})$$

$$-Aw_{11}(\theta) = H_{11}(\theta) \quad (\text{A.17})$$

$$(2i\omega_0 - A)w_{02}(\theta) = H_{02}(\theta). \quad (\text{A.18})$$

From (A.13), we get

$$\begin{aligned} u_t(\theta) &= w(z, \bar{z}, \theta) + zq(\theta) + \bar{z}\bar{q}(\theta) \\ &= w_{20}(\theta)\frac{z^2}{2} + w_{11}z\bar{z} + w_{02}(\theta)\frac{\bar{z}^2}{2} \\ &\quad + ze^{i\omega_0\theta} + \bar{z}e^{-i\omega_0\theta} + \dots \end{aligned}$$

from which $u_t(0)$, $u_t(-\tau_1)$ and $u_t(-\tau_2)$ can be determined. As We only require the coefficients of $z^2, z\bar{z}, \bar{z}^2$ and $z^2\bar{z}$, we have

$$\begin{aligned} u_t(-\tau_1)u_t(-\tau_2) &= (w(z, \bar{z}, \tau_1) + ze^{-i\omega_0\tau_1} + \bar{z}e^{i\omega_0\tau_1}) \\ &\quad \times (w(z, \bar{z}, \tau_2) + ze^{-i\omega_0\tau_2} + \bar{z}e^{i\omega_0\tau_2}) \\ &= z^2e^{-i\omega_0(\tau_1+\tau_2)} + \bar{z}^2e^{i\omega_0(\tau_1+\tau_2)} \\ &\quad + z\bar{z}(e^{-i\omega_0(\tau_1-\tau_2)} + e^{i\omega_0(\tau_1-\tau_2)}) \\ &\quad + z^2\bar{z}(e^{-i\omega_0\tau_1}w_{11}(-\tau_2) \\ &\quad + e^{-i\omega_0\tau_2}w_{11}(-\tau_1) \\ &\quad + e^{i\omega_0\tau_1}w_{20}(-\tau_2)/2) \\ &\quad + e^{i\omega_0\tau_2}w_{20}(-\tau_1)/2) + \dots \\ u_t(0)u_t(-\tau_1) &= (w(z, \bar{z}, 0) + z + \bar{z}) \\ &\quad \times u_t(-\tau_2) \\ &\quad \times (w(z, \bar{z}, \tau_1) + ze^{-i\omega_0\tau_1} + \bar{z}e^{i\omega_0\tau_1}) \\ &\quad \times (w(z, \bar{z}, \tau_2) + ze^{-i\omega_0\tau_2} + \bar{z}e^{i\omega_0\tau_2}) \\ &= z^2\bar{z}(e^{i\omega_0(\tau_1-\tau_2)} + e^{-i\omega_0(\tau_1-\tau_2)}) \\ &\quad + e^{-i\omega_0(\tau_1+\tau_2)} + \dots \\ u_t^3(-\tau_1) &= (w(z, \bar{z}, \tau_j) + ze^{-i\omega_0\tau_1} + \bar{z}e^{i\omega_0\tau_1})^3 \\ &= 3z^2\bar{z}e^{-i\omega_0\tau_1} + \dots; j \in \{1, 2\}. \\ u_t^2(-\tau_1)u_t(-\tau_2) &= (w(z, \bar{z}, \tau_1) + ze^{-i\omega_0\tau_1} + \bar{z}e^{i\omega_0\tau_1})^2 \\ &\quad \times (w(z, \bar{z}, \tau_2) + ze^{-i\omega_0\tau_2} + \bar{z}e^{i\omega_0\tau_2}) \\ &= z^2\bar{z}(e^{i\omega_0(-2\tau_1+\tau_2)} + 2e^{-i\omega_0\tau_2}) + \dots \\ u_t(-\tau_1)u_t^2(-\tau_2) &= (w(z, \bar{z}, \tau_1) + ze^{-i\omega_0\tau_1} + \bar{z}e^{i\omega_0\tau_1}) \\ &\quad \times (w(z, \bar{z}, \tau_2) + ze^{-i\omega_0\tau_2} + \bar{z}e^{i\omega_0\tau_2})^2 \\ &= z^2\bar{z}(e^{i\omega_0(-2\tau_2+\tau_1)} + 2e^{-i\omega_0\tau_1}) + \dots \end{aligned}$$

Using the above expressions, we can find the expression for other quadratic and cubic terms of u_t by substituting appropriate values for τ_1 and τ_2 .

Recall that

$$\begin{aligned}
g(z, \bar{z}) &= \bar{q}^*(0) \cdot \mathcal{F}_0(z, \bar{z}) \\
g(z, \bar{z}) &= g_{20} \frac{z^2}{2} + g_{11} z \bar{z} + g_{02} \frac{\bar{z}^2}{2} + g_{21} \frac{z^2 \bar{z}}{2} + \cdots.
\end{aligned}$$

Comparing the coefficients of z^2 , $z\bar{z}$, \bar{z}^2 , and $z^2\bar{z}$, we get

$$\begin{aligned}
g_{20} &= \bar{D}\kappa[2\xi_{xy}e^{-i\omega_0\tau_1} + 2\xi_{xz}e^{-i\omega_0\tau_2} \\
&\quad + 2\xi_{yy}e^{-2i\omega_0\tau_1} + 2\xi_{yz}e^{-i\omega_0(\tau_1+\tau_2)} \\
&\quad + 2\xi_{zz}e^{-2i\omega_0\tau_2}] \\
g_{11} &= \bar{D}\kappa[\xi_{xy}(e^{-i\omega_0\tau_1} + e^{i\omega_0\tau_1}) \\
&\quad + \xi_{xz}(e^{-i\omega_0\tau_2} + e^{i\omega_0\tau_2}) + 2\xi_{yy} \\
&\quad + \xi_{yz}(e^{-i\omega_0(\tau_1-\tau_2)} + e^{i\omega_0(\tau_1-\tau_2)}) + 2\xi_{zz}] \\
g_{02} &= \bar{D}\kappa[2\xi_{xy}e^{i\omega_0\tau_1} + 2\xi_{xz}e^{i\omega_0\tau_2} \\
&\quad + 2\xi_{yy}e^{2i\omega_0\tau_1} + 2\xi_{yz}e^{i\omega_0(\tau_1+\tau_2)} \\
&\quad + 2\xi_{zz}e^{2i\omega_0\tau_2}]. \\
g_{21} &= \bar{D}\kappa[\xi_{xy}(2w_{11}(0)e^{-i\omega_0\tau_1} + w_{20}(0)e^{i\omega_0\tau_1} \\
&\quad + 2w_{11}(-\tau_1) + w_{20}(-\tau_1)) \\
&\quad + \xi_{xz}(2w_{11}(0)e^{-i\omega_0\tau_2} + w_{20}(0)e^{i\omega_0\tau_2} \\
&\quad + 2w_{11}(-\tau_2) + w_{20}(-\tau_2)) \\
&\quad + \xi_{yy}(4w_{11}(-\tau_1)e^{-i\omega_0\tau_1} + 2w_{20}(-\tau_1)e^{i\omega_0\tau_1}) \\
&\quad + \xi_{yz}(2w_{11}(-\tau_1)e^{-i\omega_0\tau_2} + w_{20}(-\tau_1)e^{i\omega_0\tau_2} \\
&\quad + 2w_{11}(-\tau_2)e^{-i\omega_0\tau_1} + w_{20}(-\tau_2)e^{i\omega_0\tau_1}) \\
&\quad + \xi_{zz}(4w_{11}(-\tau_2)e^{-i\omega_0\tau_2} + 2w_{20}(-\tau_2)e^{i\omega_0\tau_2}) \\
&\quad + \xi_{xyy}(2e^{-2i\omega_0\tau_1} + 4) \\
&\quad + \xi_{xzz}(2e^{-2i\omega_0\tau_2} + 4) \\
&\quad + \xi_{yyz}(2e^{i\omega_0(-2\tau_1+\tau_2)} + 4e^{-i\omega_0\tau_2}) \\
&\quad + \xi_{yzz}(2e^{i\omega_0(-2\tau_2+\tau_1)} + 4e^{-i\omega_0\tau_1}) \\
&\quad + \xi_{xyz}(2e^{i\omega_0(\tau_1-\tau_2)} + 2e^{-i\omega_0(\tau_1-\tau_2)} \\
&\quad + 2e^{-i\omega_0(\tau_1+\tau_2)}) + 6\xi_{yyy}e^{-i\omega_0\tau_1} \\
&\quad + 6\xi_{zzz}e^{-i\omega_0\tau_2}]. \tag{A.19}
\end{aligned}$$

For $\theta \in [-\tau, 0)$, we have

$$\begin{aligned}
H(z, \bar{z}, \theta) &= -2\text{Re}\{\bar{q}^*(0) \cdot \mathcal{F}_0 q(\theta)\} \\
&= -g(z, \bar{z})q(\theta) - \bar{g}(z, \bar{z})\bar{q}(\theta) \\
&= -\left(g_{20}\frac{z^2}{2} + g_{11}z\bar{z} + g_{02}\frac{\bar{z}^2}{2} + \dots\right)q(\theta) \\
&\quad -\left(\bar{g}_{20}\frac{\bar{z}^2}{2} + \bar{g}_{11}z\bar{z} + \bar{g}_{02}\frac{z^2}{2} + \dots\right)\bar{q}(\theta).
\end{aligned}$$

Now using (A.15), we obtain

$$\begin{aligned}
H_{20}(\theta) &= -g_{20}q(\theta) - \bar{g}_{20}\bar{q}(\theta) \\
H_{11}(\theta) &= -g_{11}q(\theta) - \bar{g}_{11}\bar{q}(\theta).
\end{aligned}$$

From (A.7), (A.16) and (A.17), we derive the following:

$$\begin{aligned}
w'_{20}(\theta) &= 2i\omega_0 w_{20}(\theta) + g_{20}q(\theta) + \bar{g}_{02}\bar{q}(\theta), \\
w'_{11}(\theta) &= g_{11}q(\theta) + \bar{g}_{11}\bar{q}(\theta).
\end{aligned}$$

Solving the above differential equations yields

$$w_{20}(\theta) = -\frac{g_{20}}{i\omega_0}q(0)e^{i\omega_0\theta} - \frac{\bar{g}_{02}}{3i\omega_0}\bar{q}(0)e^{-i\omega_0\theta} + Ee^{2i\omega_0\theta} \quad (\text{A.20})$$

$$w_{11}(\theta) = \frac{g_{11}}{i\omega_0}q(0)e^{i\omega_0\theta} - \frac{\bar{g}_{11}}{i\omega_0}\bar{q}(0)e^{-i\omega_0\theta} + F \quad (\text{A.21})$$

for some E and F .

For $\theta = 0$, we get

$$\begin{aligned}
H(z, \bar{z}, 0) &= -2\text{Re}\{\bar{q}^* \cdot \mathcal{F}_0 q(0)\} + \mathcal{F}_0, \\
H_{20}(0) &= -g_{20}q(0) - \bar{g}_{20}\bar{q}(0) \\
&\quad + \kappa[2\xi_{xy}e^{-i\omega_0\tau_1} + 2\xi_{xz}e^{-i\omega_0\tau_2} \\
&\quad + 2\xi_{yy}e^{-2i\omega_0\tau_1} + 2\xi_{yz}e^{-i\omega_0(\tau_1+\tau_2)} \\
&\quad + 2\xi_{zz}e^{-2i\omega_0\tau_2}] \quad (\text{A.22})
\end{aligned}$$

$$\begin{aligned}
H_{11}(0) &= -g_{11}q(0) - \bar{g}_{11}\bar{q}(0) \\
&\quad + \kappa[\xi_{xy}(e^{-i\omega_0\tau_1} + e^{i\omega_0\tau_1}) \\
&\quad + \xi_{xz}(e^{-i\omega_0\tau_2} + e^{i\omega_0\tau_2}) + 2\xi_{yy} \\
&\quad + 2\xi_{yz}(e^{-i\omega_0(\tau_1-\tau_2)} + e^{i\omega_0(\tau_1-\tau_2)}) \\
&\quad + 2\xi_{zz}]. \quad (\text{A.23})
\end{aligned}$$

Using (A.7), (A.16) and (A.17), we get

$$\begin{aligned}
& \kappa \xi_y w_{20}(-\tau_1) + \kappa \xi_z w_{20}(-\tau_2) - 2i\omega_0 w_{20}(0) \\
&= g_{20}q(0) + \bar{g}_{02}\bar{q}(0) \\
&\quad - \kappa [2\xi_{xy}e^{-i\omega_0\tau_1} + 2\xi_{xz}e^{-i\omega_0\tau_2} \\
&\quad + 2\xi_{yy}e^{-2i\omega_0\tau_1} + 2\xi_{yz}e^{-i\omega_0(\tau_1+\tau_2)} \\
&\quad + 2\xi_{zz}e^{-i\omega_0\tau_2}] \tag{A.24}
\end{aligned}$$

$$\begin{aligned}
& \kappa \xi_y w_{11}(-\tau_1) + \kappa \xi_z w_{11}(-\tau_2) \\
&= g_{11}q(0) + \bar{g}_{11}\bar{q}(0) - \kappa [2\xi_{xy}e^{-i\omega_0\tau_1} \\
&\quad + 2\xi_{xz}e^{-i\omega_0\tau_2} + 2\xi_{yy}e^{-2i\omega_0\tau_1} \\
&\quad + 2\xi_{yz}e^{-i\omega_0(\tau_1+\tau_2)} + 2\xi_{zz}e^{-i\omega_0\tau_2}]. \tag{A.25}
\end{aligned}$$

Evaluate $w_{11}(0)$, $w_{20}(0)$, $w_{11}(-\tau_1)$, $w_{20}(-\tau_1)$, $w_{11}(-\tau_2)$ and $w_{20}(-\tau_2)$ using (A.20) and (A.21), and substituting in (A.24) and (A.25), we get E and F as

$$\begin{aligned}
E &= \frac{-g_{20}}{\bar{D}(\kappa \xi_y e^{-2i\omega_0\tau_1} + \kappa \xi_z e^{-2i\omega_0\tau_2} - 2i\omega_0)}, \\
F &= \frac{-g_{11}}{\bar{D}\kappa(\xi_y + \xi_z)}.
\end{aligned}$$

Thus the stability analysis of the Hopf bifurcation can now be performed using [10]. The quantities required to study the nature of the Hopf bifurcation are as follows

$$\mu_2 = \frac{-\text{Re}[c_1(0)]}{\alpha'(0)}, \quad \beta_2 = 2 \text{Re}[c_1(0)],$$

where

$$\begin{aligned}
c_1(0) &= \frac{i}{2\omega_0} \left(g_{20}g_{11} - 2|g_{11}|^2 - \frac{1}{3}|g_{02}|^2 \right) + \frac{g_{21}}{2}, \\
\alpha'(0) &= \mathbf{Re} \left(\frac{d\lambda}{d\kappa} \right)_{\kappa=\kappa_c}.
\end{aligned}$$

The direction and stability of Hopf bifurcation is determined by the sign of μ_2 and β_2 respectively. If $\mu_2 > 0$ ($\mu_2 < 0$) then the Hopf bifurcation is *super-critical* (*sub-critical*). Similarly, the bifurcating solutions are *asymptotically orbitally stable* (*unstable*) if $\beta_2 < 0$ ($\beta_2 > 0$).

References

References

- [1] A. Abuthahir and G. Raina, "Local stability and Hopf bifurcation analysis of a Rate Control Protocol with two delays", in *Proceedings of Chinese Control and Decision Conference*, 2015.

- [2] H. Balakrishnan, N. Dukkupati, N. McKeown and C.J. Tomlin, “Stability analysis of explicit congestion control protocols”, *IEEE Communications Letters*, vol. 11, pp. 823–825, 2007.
- [3] L. Baretto, “XCP-Winf and RCP-Winf: Improving Explicit Wireless Congestion Control”, *Journal of Computer Networks and Communications*, pp. 1–18, 2015.
- [4] N. Dukkupati, N. McKeown, and A. G. Fraser, “RCP-AC: Congestion control to make flows complete quickly in any environment,” in *Proceedings of IEEE INFOCOM*, 2006, pp. 1–5.
- [5] T. Dong, X. Liao and T Huang, “Dynamics of a congestion control model in a wireless access network”, *Nonlinear Analysis: Real World Applications*, vol. 14, pp. 671–683, 2013.
- [6] K. Engelborghs, T. Luzyanina and D. Roose, “Numerical bifurcation analysis of delay differential equations using DDE-BIFTOOL”, *ACM Transactions on Mathematical Software*, vol. 28, pp. 1–21, 2002.
- [7] K. Engelborghs, T. Luzyanina and G. Samaey, “DDE-BIFTOOL v. 2.00: a Matlab package for bifurcation analysis of delay differential equations”, *Technical Report TW-330*, Department of Computer Science, K.U.Leuven, Leuven, Belgium, 2001.
- [8] B. Ermentrout, *Simulating, Analyzing, and Animating Dynamical Systems: A Guide to XPPAUT for Researchers and Students*, SIAM Publications, 2002.
- [9] J.M. Harrison, *Brownian Motion and Stochastic Flow Systems*. New York: Wiley, 1985.
- [10] B.D. Hassard, N.D. Kazarinoff and Y.H. Wan, *Theory and Applications of Hopf Bifurcation*. Cambridge, U.K.: Cambridge University. Press, 1981.
- [11] L. He and H. Zhou, “Robust Lyapunov-Krasovskii based design for explicit control protocol against heterogeneous delays,” *Telecommunication Systems*, vol. 63, no. 3, pp. 377–392, Nov. 2017.
- [12] D. Katabi, M. Handley, and C. Rohrs, “Congestion control for high bandwidth-delay product networks,” *ACM SIGCOMM Computer Communication Review*, vol. 32, no. 4, pp. 89–102, Oct. 2002.
- [13] F. Kelly, G. Raina and T. Voice, “Stability and fairness of explicit congestion control with small buffers”, *ACM SIGCOMM Computer Communication Review*, vol. 38, pp. 51–62, 2008.
- [14] A. Lakshmikantha, R. Srikant, N. Dukkupati, N. McKeown and C. Beck, “Buffer sizing results for RCP congestion control under connection arrivals and departures”, *ACM SIGCOMM Computer Communication Review*, vol. 39, pp. 5–15, 2008.

- [15] K. Lei, C. Hou, L. Li and K. Xu, “A RCP-based congestion control protocol in named data networking”, in *Proceedings of International Conference on Cyber-Enabled Distributed Computing and Knowledge Discovery*, 2015.
- [16] F. Liu, Z. H. Guan and O. H. Wang, “Stability and Hopf bifurcation analysis in a TCP fluid model”, *Nonlinear Analysis: Real World Applications*, vol. 12, pp. 353–363, 2011.
- [17] F. Liu, O. H. Wang, and Z. H. Guan, “Hopf bifurcation control in the XCP for the Internet congestion control system,” *Nonlinear Analysis: Real World Applications*, vol. 13, pp. 1466–1479, 2012.
- [18] J. Liu and O.W. Yang, “Convergence, stability and robustness analysis of the OFEX controller for high-speed networks”, *Control Theory and Technology*, pp. 1–18, 2016.
- [19] M. Mahdian, S. Arianfar, J. Gibson, and D. Oran, “MIRCC: Multipath-aware ICN rate-based congestion control,” in *Proc. ACM Conf. Inform. Centric Netw.*, 2016, pp. 1–10.
- [20] N. Malangadan and G. Raina, “Rate based feedback:some experimental evaluation with NetFPGA”, *Proceedings of IEEE International Conference on Communications*, 2011.
- [21] L. Pei and Y. Wu, “Hopf bifurcation of the wireless network congestion model with state-dependent round trip delay”, *International Journal of Bifurcation and Chaos*, vol. 28, no. 9, 2018.
- [22] G. Raina, “Local bifurcation analysis of some dual congestion control algorithms”, *IEEE Transactions on Automatic Control*, vol. 50, pp. 1135–1146, 2005.
- [23] Y. Ren, J. Li, S. Shi, L. Li, and G. Wang, “An explicit congestion control algorithm for Named Data Networking,” in *Proc. IEEE INFOCOM*, 2016, pp. 294–299.
- [24] N.K. Sharma, A. Kaufmann, T.E. Anderson, A. Krishnamurthy, J. Nelson and S.Peter, “Evaluating the Power of Flexible Packet Processing for Network Resource Allocation”, in *USENIX Symposium on Networked Systems Design and Implementation*, 2017.
- [25] R. Srikant, *The Mathematics of Internet Congestion Control*. Birkhauser, 2004.
- [26] G. Stépán, *Retarded dynamical systems: stability and characteristic functions*. Essex: Longman Scientific & Technical, 1989.
- [27] S.H. Strogatz, *Nonlinear dynamics and chaos: with applications to physics, biology, chemistry, and engineering*, CRC Press, 2018.

- [28] Y.D. Sun, Z.Z. Ji and H. Wang, “Towards Performance Evaluation of Rate Control Protocol in Satellite Networks”, *International Journal of Electrical and Computer Sciences*, vol. 12, pp. 37–41, 2012.
- [29] T. Voice and G. Raina, “Stability analysis of a max-min fair Rate Control Protocol (RCP) in a small buffer regime”, *IEEE Transactions on Automatic Control*, vol. 54, pp. 1908–1913, 2009.
- [30] J. Wang, P. Dong, J. Chen, J. Huang, S. Zhang and W. Wang, “Adaptive explicit congestion control based on bandwidth estimation for high bandwidth-delay product networks”, *Computer Communications*, vol. 30, pp. 1235–1244, 2013.
- [31] B. Wydrowski and M. Zukerman, “MaxNet: A congestion control architecture,” *IEEE Communication Letters*, vol. 6, no. 11, pp. 512–514, Nov. 2002.
- [32] L. Zhang, D. Estrin, J. Burke, V. Jacobson, J.D. Thornton, D.K. Smetters, B. Zhang, G. Tsudik, D. Massey and C. Papadopoulos, “Named Data Networking (NDN) project,” PARC, Technical Report NDN-0001, Oct. 2010.
- [33] Y. Zhang, D. Leonard, and D. Loguinov, “JetMax: Scalable max-min congestion control for high-speed heterogeneous networks,” *Computer Networks*, vol. 52, no. 6, pp. 1193–1219, Apr. 2008.
- [34] S. Zhang and J. Xu, “Quasiperiodic motion induced by heterogeneous delays in a simplified Internet congestion control model”, *Nonlinear Analysis: Real World Applications*, vol. 14, pp. 661–670, 2013.
- [35] S. Zhong, Y. Liu, J. Li, and K. Lei, “A Rate-Based Multipath-Aware Congestion Control Mechanism in Named Data Networking,” in *Proceeding of IEEE International Symposium on Ubiquitous Computing and Communications*, 2017.

